Linear Ladder-Type π-Conjugated Polymers Composed of Fused Thiophene Ring Systems

Kenichi Oyaizu, Tomokazu Iwasaki, Yoshiaki Tsukahara, and Eishun Tsuchida*

Advanced Research Institute for Science and Engineering, Waseda University, Tokyo 169-8555, Japan

Received October 10, 2003

ABSTRACT: A novel carbon−sulfur (C_2S) analogue of polyacene has been synthesized and characterized. The polymer is composed of a nondegenerate trans−cisoid polyacetylene backbone in which all hydrogen atoms are replaced with sulfur atoms to form thiophene rings that are fused into a linear cross-conjugated ladder-type structure. The newly developed synthetic route of the ladder-type polymer is based on an intramolecular condensation of a prepolymer consisting of 3-(alkane-1-sulfinyl)thiophen-2,5-diyl units in triflic acid. The geometric and band electronic structure of the ladder-type polymer were calculated and analyzed at the PM5 level of theory. The fused ring structure imposes strong quinonoid-type character to the originally benzenoid polyene backbone, which destabilizes the HOMO and stabilizes the LUMO and thus reduces the band gap. The shift of absorption and emission maxima to longer wavelengths responding to lower $\pi-\pi^*$ transition energies than those of polythiophene and the smaller gap between electrochemical p- and n-doping potentials are consistent with the reduction of the band gap. The microstructure of the isolated oligomers in their neutral, singly oixidzed, and doubly oxidized states were computed for short and intermediate chain length. Various energetic and structural aspects of the convergence behavior from the properties of small cations or dications to those of an isolated polaronic or bipolaronic defects on a sufficiently long chain were monitored and are discussed. The geometric structures of the p-doped ladder-type polymer in the form of either polaron or bipolaron were calculated by adopting suitable boundary conditions to represent charged unit cells. The geometry relaxation process for the charged ladder-type backbone induces the appearance of a stronger quinonoidic character than that in the case of polythiophene, which suggests that the fused rings more easily adopt quinonoid forms than thiophene rings. Calculated energetic aspects of the doping behavior and the paramagnetic resonance spectra of p-doped polymers revealed that the ladder-type polymer possesses polaron as the prevailing charged species, in contrast to many other π-conjugated polymers where bipolaron is the lowest-energy charge storage configuration.

1. Introduction

Linear π-conjugated polymers such as polyacetylene are subject to Peierls distortion[1] and are predicted to possess band gaps that depend on the degree of bond length alternation along the polymer backbone. Although band gap and bond alternation are not linearly correlated, it is important to reduce the bond length alternation for the band gap reduction of one-dimensional polymers.[2] Because of the environmental stability,[3] the relatively small band gap (≈2.0 eV),[4,5] and the structural versatility, polythiophene (**PT**) has been widely used as a backbone to construct low band-gap polymers.[6,7] Since polythiophene is based on a *cis*-polyacetylene backbone which is nondegenerate in the ground state, two limiting structures, benzenoid and quinonoid structures, can exist as indicated in Chart 1a.[8] Actual polythiophene derivatives have geometries between the two limiting structures, depending on the extent of their contribution. A quinonoid form of polythiophene with $\delta r = 0.06$ Å is predicted to possess a near-zero band gap.[9] Here δr is defined as the average value of the bond length alternation along the backbone of the polymer. Therefore, a potential way to design a low band-gap polythiophene is to modify the chemical structure toward a quinonoid form.

Polythieno[3,4-*b*]benzene is the first known derivative of polythiophene which has a low band gap (1.0−1.2 eV) without doping.[10−14] It is known that the nodal pattern of the highest occupied molecular orbital (HOMO) in heteroaromatic oligomers is characteristic of the benzenoid form while that of the lowest unoccupied molecular orbital (LUMO) is characteristic of the quinonoid form.[15,16] Brédas et al. rationalized that fusion of a benzene ring to thiophene effectively increased the quinonoid contribution to the electronic structure, by destabilizing the HOMO and stabilizing the LUMO, which decreased the band gap.[17,18] A large number of studies have been stimulated in search of low band-gap polymers, with the introduction of fused ring systems such as thieno[3,4-*b*]pyrazine[19] and tricyclic thiophenes such as [1,2,5]thiadiazolo[3,4-*b*]thieno[3,4-*e*]pyrazine and dithieno[3,4-*b*;3′,4′-*e*]pyrazine.[20] Polythiophenes, which involve as units the fused oligothiophenes, have also been studied, such as polythieno[3,4-*b*]thiophene[8,21−23] and poly(dithieno[3,4-*b*;3′,4′-*d*]thiophene).[24] However, these polymers possess $C_\alpha-C_{\alpha'}$ (or $C_\alpha-C_{\beta'}$[25])

Chart 1. Limiting Structures for Polythiophene (PT) and Ladder-type Polythiophene (LPT)

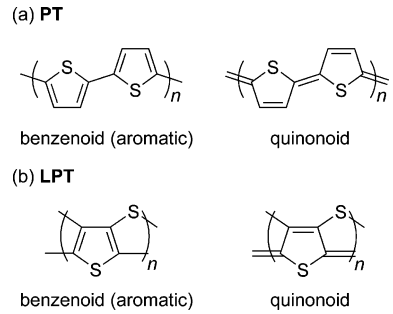

* Corresponding author: Telephone: +81-3-5286-3120. Fax: +81-3-3205-4740. E-mail: eishun@waseda.jp.

10.1021/ma030520p CCC: $27.50
Published on Web 01/21/2004

Chart 2. *x*-Mer Oligothiophene (T_x) and Fused Oligothiophene (FT_x) Models for PM5 Calculations

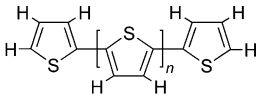

T_x : $n = x-2$
(T_1 = thiophene)

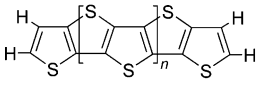

FT_x : $n = x-2$

single bonds to connect the fused rings, and band-gap values reported so far are not small enough to allow metallic conduction without dopants.[26]

A linear ladder-type polymer **LPT** (Chart 1b) in which $C_\alpha-C_{\alpha'}$ bonds are involved in cross-conjugated thiophene rings may be viewed as an unprecedented carbon−sulfur (C_2S) analogue of polyacene. The fused thiophene rings in **LPT** are considered to be almost coplanar, which is preferable for the band-gap reduction of π-conjugated systems. Recently, Rajca et al. reported the synthesis of an isomeric heptamer by the condensation of [3,3′]bi[dithieno[2,3-*b*;3′,2′-*d*]thiophenyl] derivatives.[27] However, the rigid backbone of the product was not linear but annealed into a helix, because thiophene rings were inevitably arranged in a fashion that they pointed the same direction.[27]

In this paper, we report the first synthesis of a linear **LPT** by the polymer-analogous condensation[28−32] of regioregular (head-to-tail) poly[3-(alkane-1-sulfinyl)-thiophene], and the oligomers containing up to five fused rings. We will also calculate and qualitatively analyze the band electronic and geometric structures of **LPT** at the PM5 level of theory[33] and compare them to the structures of **PT**. We will first perform geometry optimizations of oligomer models in Chart 2, and then calculate the geometric and band electronic structures of the polymers. We found that, while the benzenoid-type structure is dominant in the ground state of **PT**, quinonoid characters can be strongly imposed on **LPT**. Calculated band gap values and experimental data will be discussed in view of geometrical changes imposed by the fused thiophene rings. In Chart 2, a benzenoid bond alternation pattern is drawn for $\mathbf{FT_x}$ but this picture needs improvement due to the quinonoid-type characters imposed by the fused framework.

Another important issue is the microstructure of the doped materials in terms of bond length and angles and, in particular, the spatial extension and the structural properties of the charged defects in the form of either polarons or bipolarons. It has been shown that **PT** is subject to structural modifications toward bipolaronic quinonoid forms upon charge transfer as shown in Chart 3a.[15] In this paper, we report the results of PM5 calculations on the structure of short-chain and of extended oligomers $\mathbf{FT_x}$ in their singly and doubly oxidized states with *x* ranging from 3 to 9. These cation radicals and dications are models for isolated, singly and doubly charged defects, respectively, on an otherwise unperturbed oligothiophene chain and may serve as an approximation to the actual defect structure encountered in the p-doped **LPT**. The evolution of the structures of these charged species with increasing chain length will be monitored in order to assess the proper-

Chart 3. Structure of Charged Defects in Doped PT and LPT

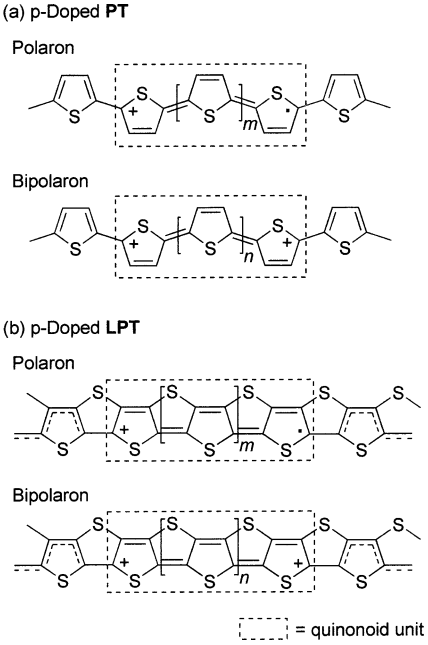

ties of idealized, isolated charged defects on the polymer backbone. We will then calculate the geometric structures of **LPT** and **PT** in the oxidized states by adopting sufficient distances of translation vectors to accommodate the +1 or +2 charge per unit cell, taking into account the spatial extension of the charged defects in the oligomer models. The geometry relaxation process for the charged **LPT** backbone induces the appearance of an even stronger quinonoidic character than that of **PT**, which suggests that the coplanar thiophene rings in **LPT** more easily adopt quinonoid forms as shown in Chart 3b. Interestingly, calculated energetic aspects of the doping behavior and the spectroscopic results indicate that polaron is favored over bipolaron as a charge carrier in **LPT**, even at fairly high doping levels.

2. Computational Methods

2.1. Optimization of Neutral States. We calculated the structures of the periodic linear π-conjugated system **LPT** and its oligomer models $\mathbf{FT_x}$ that involve as units the fused thiophene rings. We also calculated the structures of poly- (**PT**) and oligothiophene ($\mathbf{T_x}$) as the control compounds. In **PT** and $\mathbf{T_x}$, the adjacent monomer units were arranged in a fashion that they pointed in opposite directions. Although we did not limit our theoretical investigation to a planar conformation, the converged structures of **PT** and $\mathbf{T_x}$ showed nearly coplanar geometries for thiophene rings. This was consistent with the results of previous calculations at higher theory levels,[34] showing that s-trans coplanar structures were the most stable in energy. In this work, we mainly investigated oligothiophenes ($\mathbf{T_x}$) containing an odd number of thiophene rings ($x = 1, 3, 5, 7, 9, 11$) and fused oligothiophenes ($\mathbf{FT_x}$) containing an odd number of fused rings ($x = 2, 3, 4, 5, 6, 7, 8, 9, 10, 11$) (Chart 1) and thus both presenting C_{2v} symmetry. However, no symmetry constraint was applied on the oligomer models, considering that the spatial extension of the charged defects along the chain could be asymmetric. The terminal groups can be chosen (−H for benzenoid and $=CH_2$ for quinonoid forms[35]) to deter-

mine the structures of the ground state of the oligomer with respect to a benzenoid or quinonoid type. We used oligomer models terminated by −H throughout this work, with a view to extend the calculation to polymer models. Geometry optimizations of the oligomer models were performed using the PM5 method[33] that has been successfully applied to predicting the molecular structures of organic compounds. The WinMOPAC 3.5 program package from Fujitsu Co. was used for the PM5 calculations.

Polymer models (**PT** and **LPT**) were constructed using translation vectors to represent boundary conditions along the chain. Polymer models with insufficient crystal lattice size can lead to erroneous results in certain cases. We concluded that the unit cell containing 24 carbon atoms (6 thiophene rings for **PT** and 12 fused rings for **LPT**) were long enough to estimate the structures of the infinite chain. Calculated structures of $\mathbf{FT_{11}}$ and $\mathbf{FT_{10}}$ were somewhat different from those of $\mathbf{FT_2}$ and $\mathbf{FT_3}$, but were very similar to those of $\mathbf{FT_6}$, most of the differences between the corresponding bond lengths being within 0.0002 Å. Therefore, initial geometrical parameters to calculate the polymer structures were taken from those for the middle rings of the corresponding 11-mers. Sufficiently large unit cells containing 48 carbon atoms (12 thiophene rings for **PT** and 24 fused rings for **LPT**) were employed for the band calculation, which were constructed using the WinMAKPOL program from Fujitsu Co. The electronic structures were obtained by performing PM5 geometry optimizations followed by band calculations. The WinBZ program involved in the WinMOPAC 3.5 package was used for the band calculation. After the geometry optimization, the distances of the translation vectors were 46.3 and 46.1 Å for **PT** and **LPT**, respectively.

It is known that Hartree−Fock calculations without correcting the electron correlation effects generally overestimate the band gap (E_g) of polymers. In previous reports, the calculated band gap values for **PT** were $E_g^{calc} = 6.04$ eV at the PM3 level[36] and 5.9 eV at the ab initio STO-3G level[37] which were extrapolated from HOMO−LUMO energy differences for oligomers, and 8.14 eV using ab initio Hartree−Fock crystal orbital theory.[38,39] A number of methods have been reported to improve the agreement with the experimental data ($E_g^{exp} = 2.1$ eV),[40] such as the nonempirical valence effective Hamiltonian (VEH) method ($E_g^{calc} = 1.6-1.8$ eV)[41] and the modified extended Hückel method ($E_g^{calc} = 2.05$ eV).[20] In the present report, the absolute values for the calculated band gaps did not have significance because we did not include electron correlation. However, observed qualitative trends sufficed to provide insights into the difference between the electronic states of **LPT** and **PT**.

2.2. Optimization of Oxidized States. Karpfen et al. investigated the evolution of and the convergence to the structural properties of bipolaronic defect in oligothiophene up to 21-mers at the SCF 3-21G* level with the aid of semiempirical methods such as PM3, and found that the computed C−C and C−S bond lengths were sensitive to double ionization.[42] Brédas et al. calculated the optimized C−C bond lengths of 11-mers in the neutral, singly oxidized, and doubly oxidized states at the AM1 level, to discuss the spatial extension of polaronic and bipolaronic defects.[43] In these reports, the upper limits to the polaronic and bipolaronic defects on the oligothiophene chain were estimated at 5 and 9 thiophene rings (i.e., 20 and 36 C−C bonds), respectively.[42,43]

In the present study, we first calculated the geometries of oxidized oligomers ($\mathbf{FT}_x^{n+}$ and $\mathbf{T}_x^{n+}$) at the PM5 level, and then extended the calculation to oxidized polymers. We performed geometry optimizations according to the previously outlined procedure,[42,43] and restricted the discussion to the behavior of the C−C bond lengths. While the neutral as well as the dicationic oligomers were treated as closed-shell systems, singly oxidized oligomers (cation radicals) were calculated as open-shell systems at the RHF level. The structures of the cation radicals ($\mathbf{FT}_x^{+}$ and $\mathbf{T}_x^{+}$) and the dications ($\mathbf{FT}_x^{2+}$ and $\mathbf{T}_x^{2+}$) with x ranging from 3 to 9 were optimized. While the structures of long dications up to $x = 21$ could be optimized, cation radicals with x larger than 9 could not be treated at the PM5 level because of restrictions in the available computing resources.

The oxidized states of the polymers were treated as follows. A charge of +1 (cation radical) was allocated ($Q^{cell} = +1$) to a unit cell containing x carbon atoms ($N_C^{cell} = x$), and a one-dimensional polymer was generated from the unit cell by a translation vector along the chain. Within the chain, the coupling of adjacent two cation radicals to form a dication across the cell boundary was forbidden, because the positions of the charged defect were also subjected to the translation gliding along the chain. As a result, each optimized cell accommodated a semiquinonoidal defect and the system realized the polaron state. The doping level can be defined as $y_C = Q^{cell}/N_C^{cell} = +1/x$ (i.e., the amount of charge per number of carbon atoms in the unit cell). Conventional representation of the doping level y_π,[44,45] i.e., the amount of charge per π electrons, was not used in this study, because of the difference between the number of π electrons per repeating unit for **LPT** (8π e$^-$) and **PT** (6π e$^-$). We may note in passing that both **LPT** and $\mathbf{FT}_x$ molecules constitute aromatic systems with $4n + 2$ π electrons in the ground state.

When the unit cell accommodated a charge of $Q^{cell} = +2$ (dication), the system realized the bipolaron state with the doping level of $+2/x$. We could change the doping level by varying the size of the unit cell (x). Thus, we could calculate the polaron state and the bipolaron state at the same doping level ($+1/x$) by doubling the size of the unit cell for the bipolaron state (i.e., $y_C = +2/2x = +1/x$).

Calculation of very heavily doped polaron states could be invalid, because the present computational method premised that the polaronic semiquinonoidal defect was isolated in the unit cell. Optimized geometries with sufficiently large cell sizes indicated that the semiquinonoidal defect extended over ca. 24 carbon atoms. Therefore, unit cells with less than 24 carbon atoms were too small to accommodate the polaronic defect, and accordingly the highest doping level that could be treated in this study was $y_C = +1/24$ (= 0.042). On the other hand, geometries of polymers at very low doping levels ($y_C < +1/48$) could not be optimized, because the unit cells with more than 48 carbons were too large to undergo calculation. As a result, doped polymer models for calculation ranged in y_C from +1/48 to +1/24. Very fortunately, most of the experimentally determined doping levels for the polymers synthesized in this study were in this range.

Although the transition state for the polaron−polaron coupling process could not be followed, we could learn

energetic aspects of the coupling process from the heat of formation calculated for a unit cell in the polaron state and that in the bipolaron state at the same doping level. The propriety of this treatment is discussed in this paper.

3. Materials and Measurements

3.1. Materials. See the Supporting Information for the preparative methods for 3-decylsulfanyl-5,5′-dimethyl-[2,2′]-bithiophenyl (**DS-T$_2$**), 3,4′-bis(decylsulfanyl)-5,5”-dimethyl-[2,2′;5′,2”]terthiophene (**DS-T$_3$**), poly(3-decylsulfanylthiophene) (**DS-PT**), and poly[3-(1-methylheptylsulfanyl)thiophene] (**MS-PT**). Poly(3-hexylthiophene) (**H-PT**) was prepared from 2-bromo-3-hexylthiophene by the conventional Grignard coupling method.[46−48] All solvents were purified by distillation prior to use. Tetrabutylammonium tetrafluoroborate [(TBA)BF_4] was obtained from Tokyo Kasei Co., and recrystallized twice from benzene/ethyl acetate. All other regents were obtained from Kanto Chemical Co. or Tokyo Kasei Co. and used without further purification.

3-(Decane-1-sulfinyl)-5,5′-dimethyl-[2,2′]bithiophenyl (DSO-T$_2$). A mixture of **DS-T$_2$** (0.20 g, 0.57 mmol) in CH_2Cl_2 (40 mL), an aqueous solution of hydrogen peroxide (30%, 8 mL), and acetic acid (2 mL) was stirred at 30 °C for 3 h. The organic layer was extracted with $CHCl_3$, and the extract was washed with water. Dehydration of the extract followed by evaporation of the solvent gave the product as a yellow powder (0.21 g, 0.52 mmol). Yield: 92%. ^{1}H NMR ($CDCl_3$, 500 MHz, ppm): δ 7.19 (s, 1H), 6.86 (d, J = 3.4 Hz, 1H), 6.58 (d, J = 3.5 Hz, 1H), 2.97−2.74 (m, 2H), 2.46 (s, 3H), 2.40 (s, 3H), 1.58, 1.33, 1.18, 0.87 (m, 19H). ^{13}C NMR ($CDCl_3$, 125 MHz, ppm): δ 140.0, 139.6, 138.6, 137.0, 133.7, 125.9, 124.1, 118.5, 55.7, 31.8, 29.4, 29.3, 29.2, 29.1, 28.9, 28.7, 23.7, 22.6, 15.3, 14.1. MS (EI, m/z): calcd for M^+ 382.66; found 382. IR (KBr, cm^{-1}): 1052 ($\nu_{S=O}$), 834 (δ_{C-H}). Anal. Calcd for $C_{20}H_{30}OS_3$: C, 62.78; H, 7.90. Found: C, 63.25; H, 8.59.

4-Decyl-2,6-dimethyldithieno[3,2-*b*;2′,3′-*d*]thiophen-4-ium Triflate (D-Me$_2$FT$_2$). DSO-T$_2$ was dissolved in triflic acid (16 mL), and the resulting solution was stirred at 80 °C for 24 h. After cooling, the solution was poured into diethyl ether (500 mL) to precipitate the product which was collected by filtration, washed with diethyl ether, and dried under vacuum to give a pale brown powder (0.39 g, 0.76 mmol). Yield: 95%. ^{1}H NMR (DMSO-d_6, 500 MHz, ppm): δ 7.66 (s, 2H), 4.15 (t, J = 7.2 Hz, 2H), 2.76 (s, 6H), 1.64, 1.38, 1.27, 0.88 (m, 19H). ^{13}C NMR (DMSO-d_6, 125 MHz, ppm): δ 166.7, 131.6, 131.2, 128.4, 67.3, 38.1, 29.7, 29.5, 29.5, 29.3, 29.1, 28.6, 22.7, 15.3, 14.1. IR (KBr, cm^{-1}): 1259, 794 (ν_{C-F}), 1157 (ν_{SO3}), 839 (δ_{C-H}). Anal. Calcd for $C_{21}H_{29}F_3O_3S_4$: C, 49.00; H, 5.68. Found: C, 48.23; H, 6.32.

2,6-Dimethyldithieno[3,2-*b*;2′,3′-*d*]thiophene (Me$_2$FT$_2$). D-Me$_2$FT$_2$ (0.21 g, 0.4 mmol) was dissolved in pyridine (15 mL), and the resulting solution was refluxed for 24 h with constant stirring. After cooling, the solution was poured into hydrochloric acid (200 mL). The pale brown precipitate was collected by filtration, washed with water, and dried under vacuum to give the product (0.09 g, 0.39 mmol). Yield: 97%. ^{1}H NMR (CD_2Cl_2, 500 MHz, ppm): δ 7.01 (s, 2H), 2.48 (s, 6H). MS (EI, m/z): calcd for M^+ 224.37; found 224. IR (KBr, cm^{-1}): 845 (δ_{C-H}). Anal. Calcd for $C_{10}H_8S_3$: C, 53.05; H, 3.56. Found: C, 53.10; H, 3.87.

3,4′-Bis(decane-1-sulfinyl)-5,5”-dimethyl-[2,2′;5′,2”]terthiophene (DSO-T$_3$). According to the procedure essentially identical with the preparation of **DSO-T$_2$**, **DSO-T$_3$** was prepared from **DS-T$_3$** (0.31 g, 0.50 mmol) by the oxidation of the decylsulfanyl group at 30 °C for 8 h. The product was obtained as a yellow powder (0.30 g, 0.46 mmol). Yield: 95%. ^{1}H NMR ($CDCl_3$, 500 MHz, ppm): δ 7.46 (s, 1H), 7.34 (s, 1H), 7.02 (d, J = 3.5 Hz, 1H), 6.69 (d, J = 3.5 Hz, 1H), 2.99 (m, J = 8.8 Hz, 4H), 2.59 (s, 3H), 2.50 (s, 3H), 1.74, 1.43, 1.25, 0.87 (m, 38H). ^{13}C NMR ($CDCl_3$, 125 MHz, ppm): δ 140.0, 139.6, 138.6, 137.0, 133.7, 125.9, 124.1, 118.5, 55.7, 31.8, 29.4−28.7, 23.7, 22.6, 15.3, 14.1. MS (EI, m/z): calcd for M^+ 653.11; found 653. IR (KBr, cm^{-1}): 1050 ($\nu_{S=O}$), 828 (δ_{C-H}). Anal. Calcd for $C_{34}H_{52}O_2S_5$: C, 62.53; H, 8.03. Found: C, 62.01; H, 8.98.

2,6-Dimethyl-8,9-didecyl-3,4,5-trithia-8,9-dithioniacyclopenta[1,2-*a*;4,3-*a*′]dipentalene Triflate (D-Me$_2$FT$_3$). According to the procedure essentially identical with the preparation of **D-Me$_2$FT$_2$**, **D-Me$_2$FT$_3$** was prepared from **DSO-T$_3$** (0.13 g, 0.20 mmol). The product was obtained as a pale brown powder (0.17 g, 0.19 mmol). Yield: 95%. ^{1}H NMR (DMSO-d_6, 500 MHz, ppm): δ 7.72 (s, 2H), 4.24 (m, J = 8.6 Hz, 4H), 3.17 (s, 6H), 1.68, 1.37, 1.27, 0.88 (m, 38H). ^{13}C NMR (DMSO-d_6, 125 MHz, ppm): δ 173.0, 156.5, 145.2, 144.8, 129.8, 123.2, 76.6, 43.9, 31.6−27.0, 25.7, 18.4, 14.3, 13.9. IR (KBr, cm^{-1}): 1251, 786 (ν_{C-F}), 1150 (ν_{SO3}), 826 (δ_{C-H}). Anal. Calcd for $C_{36}H_{50}F_6O_6S_7$: C, 47.14; H, 5.49. Found: C, 48.11; H, 5.72.

2,6-Dimethyl-3,4,5,8,9-pentathiacyclopenta[1,2-*a*;4,3-*a*′]dipentalene (Me$_2$FT$_3$). According to the procedure essentially identical with the preparation of **Me$_2$FT$_2$**, **Me$_2$FT$_3$** was prepared from **D-Me$_2$FT$_3$** (0.092 g, 0.10 mmol). The product was obtained as a pale brown powder (0.033 g, 0.098 mmol). Yield: 98%. ^{1}H NMR (CD_2Cl_2, 500 MHz, ppm): δ 7.05 (s, 2H), 2.48 (s, 6H). Anal. Calcd for $C_{14}H_8S_5$: C, 49.96; H, 2.40. Found: C, 49.22; H, 2.97.

Poly[3-(decane-1-sulfinyl)thiophene] (DSO-PT). To a solution of **DS-PT** (0.12 g, 0.44 mmol unit) in CH_2Cl_2 (14 mL) was slowly added an aqueous solution of hydrogen peroxide (30%, 2.4 mL) and acetic acid (1 mL). After stirring at 30 °C for 15 h, the resulting mixture was poured into methanol/water (v/v = 1/1) to precipitate the product which was collected by filtration and dried under vacuum to give **DSO-PT** as a red powder (0.11 g, 0.39 mmol unit). Yield: 89%. ^{1}H NMR ($CDCl_3$, 500 MHz, ppm): δ 7.69 (s, 1H), 3.10, 2.90 (m, 2H), 1.80, 1.68, 1.65, 1.45, 1.25, 0.92 (m, 19H). ^{13}C NMR ($CDCl_3$, 125 MHz, ppm): δ 173.2, 142.4, 126.3, 126.1, 56.5, 31.9, 29.9, 29.8, 29.7, 29.5, 29.4, 28.9, 22.8, 14.3. GPC (THF, polystyrene standard): M_n = 6200, M_w = 7500 (M_w/M_n = 1.2). UV−vis ($CHCl_3$, nm): λ_{max} = 468 nm. IR (KBr, cm^{-1}): 1058 ($\nu_{S=O}$), 723 (δ_{C-H}). Anal. Calcd for $C_{14}H_{22}OS_2$: C, 62.17; H, 8.20. Found: C, 62.09; H, 8.01.

Poly[3-(1-methylheptane-1-sulfinyl)thiophene] (MSO-PT). According to the procedure essentially identical with the preparation of **DSO-PT**, **MSO-PT** was prepared from **MS-PT** (0.030 g, 0.13 mmol unit). The product was obtained as a dark red powder (0.027 g, 0.11 mmol unit). Yield: 81%. ^{1}H NMR ($CDCl_3$, 500 MHz, ppm): δ 7.66 (s, 1H), 3.22, 2.93 (m, 1H), 1.80, 1.48, 1.28, 0.89 (m, 16H). ^{13}C NMR ($CDCl_3$, 125 MHz, ppm): δ 165.2, 143.0, 127.6, 126.5, 59.6, 37.9, 31.9, 29.5, 27.7, 26.4, 22.4, 14.4. GPC (THF, polystyrene standard): M_n = 5400, M_w = 7600 (M_w/M_n = 1.4). UV−vis ($CHCl_3$, nm): λ_{max} = 454 nm. IR (KBr, cm^{-1}): 1052 ($\nu_{S=O}$), 722 (δ_{C-H}). Anal. Calcd for $C_{12}H_{18}OS_2$: C, 59.46; H, 7.49. Found: C, 58.97; H, 7.31.

The Ring-Closed Product from DSO-PT (D-LPT). A solution of **DSO-PT** (0.095 g, 0.50 mmol unit) in CH_2Cl_2 (2 mL) was added dropwise to triflic acid (20 mL) with constant stirring. The solution was warmed to 60 °C and stirred for 1 h to remove CH_2Cl_2. The resulting solution of **DSO-PT** in triflic acid was stirred at 80 °C for 24 h to undergo the ring-closing reaction. The reaction was quenched by pouring the mixture into diethyl ether (300 mL) to precipitate the product. The precipitate was collected by filtration and dried under vacuum to give **D-LPT** as a dark brown powder (0.20 g). Yield: 96%. ^{1}H NMR (DMSO-d_6, 500 MHz, ppm): δ 3.64 (m, 2H), 1.37, 0.88 (m, 19H). IR (KBr, cm^{-1}): 1153, 1356 (ν_{SO3}), 753 (δ_{C-H}), 636 (ν_{C-F}). UV−vis ($CHCl_3$, nm): λ_{max} = 569 nm. Anal. Calcd for $C_{15}H_{21}F_3O_3S_3$: C, 44.76; H, 5.26. Found: C, 44.02; H, 5.11.

The Ring-Closed Product from MSO-PT (M-LPT). According to the procedure essentially identical with the preparation of **D-LPT**, **M-LPT** was prepared from **MSO-PT** (0.025 g, 0.11 mmol unit). The product was obtained as a dark red powder (0.036 g, 0.10 mmol unit). Yield: 90%. ^{1}H NMR (DMSO-d_6, 500 MHz, ppm): δ 3.50 (m, 1H), 2.10, 1.72, 1.20, 0.93 (m, 16H). IR (KBr, cm^{-1}): 1169, 1389 (ν_{SO3}), 714 (δ_{C-H}), 646 (ν_{C-F}). UV−vis ($CHCl_3$, nm): λ_{max} = 536 nm. Anal. Calcd for $C_{13}H_{17}F_3O_3S_3$: C, 41.70; H, 4.58. Found: C, 40.99; H, 4.32.

Ladder-Type Polythiophene (LPT). The ring-closed polymer, **M-LPT**, was converted to **LPT** by treatment with pyridine as follows. A suspension of **M-LPT** (0.035 g, 0.093 mmol unit) in pyridine (15 mL) was refluxed for 24 h. After

cooling, the mixture was poured into methanol containing 20% hydrochloric acid. The resulting precipitate was collected by filtration, washed with methanol and water, and dried under vacuum to give **LPT** as a dark red powder (0.010 g, 0.091 mmol unit). Yield: 98%. CP/MAS (500 MHz, ppm): δ 135. Anal. Calcd for C_4S_2: C, 42.83. Found: C, 42.88; H, 0.01. An essentially identical result was obtained by the dealkylation of λ^4-decylsulfanyliumdiyl groups in **D-LPT**. An **LPT**-coated glassy carbon disk electrode for voltammetric experiments was prepared in situ by the dealkylation of the λ^4-(1-methyl)-heptylsulfanyliumdiyl groups in **M-LPT** as a film on the electrode, which was prepared by spin-casting the solution of **M-LPT** in $CHCl_3$.

3.2. Measurements. ^{1}H and ^{13}C NMR spectra were recorded on a JEOL JNM-LA500 (500 MHz ^{1}H, 125 MHz ^{13}C) spectrometer with chemical shifts downfield from tetramethylsilane as the internal standard. ^{13}C CP/MAS spectra were obtained using a JEOL GSX-400 spectrometer. Infrared spectra were obtained using a Jasco FT-IR 410 spectrometer with potassium bromide pellets. UV−vis spectra were recorded using a JASCO V-550 spectrometer. Photoluminescence spectra were recorded using a Hitachi F-4500 spectrometer. Molecular weight measurements were done by gel permeation chromatography (GPC) using a TOSOH LS-8000 instrument. THF was used as an eluent. Calibration was done with polystyrene standards. Elemental analyses were performed using a Perkin-Elmer PE−2400 II and a Metrohm 645 multi-DOSIMAT. Two parallel analyses were performed for each sample. Mass spectra were obtained using a Shimadzu GCMS-QP5050 spectrometer. Electrochemical measurements were carried out in a conventional two-compartment cell. A 6 mm diameter glassy carbon disk was used as a working electrode and polished before each experiment with 0.05 μm alumina paste. The auxiliary electrode, a coiled platinum wire, was separated from the working solution by a fine-porosity frit. The reference electrode was a commercial Ag/AgCl immersed in a solution of 0.1 mol/L $TBABF_4$ in CH_3CN, which was placed in the main cell compartment. The formal potential of the ferrocene/ferrocenium couple was 0.55 V vs this Ag/AgCl electrode. All potentials are quoted with respect to this reference electrode. A Nikko Keisoku DPGS-1 dual potentiogalvanostat and a Nikko Keisoku NFG-3 universal programmer were employed with a Graphtec WX2400 X-Y recorder to obtain the voltammograms. ESR spectra were recorded using a JEOL TE−200 spectrometer with a 100 kHz field modulation frequency and a 0.1 mT width.

4. Results and Discussion

4.1. Optimized Structures in Neutral States. The PM5-optimized geometric structures of $\mathbf{T}_x$ and $\mathbf{FT}_x$ in their neutral states showed that all the inner thiophene rings presented the same geometry, which slightly differed from that found in the outer units due to the chain-end effects. We present in Figure 1a how the bond alternation converged with increasing x concerning the central moieties, and in Figure 1b the optimized structures of the 11-mers. The bond lengths of $\mathbf{FT}_x$ were characterized by a much smaller degree of C−C bond alternation δr (= $R(C_1-C_2) - R(C_2-C_3)$) on the order of 0.005 Å than those of $\mathbf{T}_x$ which were on the order of 0.073 Å. The structure of $\mathbf{T}_x$ showed a clear benzenoid-type character. We note that high-level ab initio calculations[49,50] are also indicative of the degree of bond alternation of 0.07 Å for the rings in $\mathbf{T}_x$ and **PT**. The smaller bond alternation in $\mathbf{FT}_x$ was related to an enhanced quinonoid character of the rings. Therefore, the fused thiophene rings successfully imposed quinonoid-type characteristics on the main chain.

We show in Figure 2 the crystal orbitals of **LPT** and **PT** in the frontier orbital region, together with their band electronic structures. The HOCO (the highest occupied crystal orbital) and the LUCO (the lowest unoccupied crystal orbital) consisted of the p_z-orbitals vertical to the molecular plane. It is known that the HOCO of **PT** has nodes passing through the sulfur atoms and looks like an alternation of segments of the HOCO of trans−cisoid polyacetylene.[20,40,41,51,52] Similarly, the HOCO of **LPT** did not include any contribution from the sulfur atoms. On the other hand, the LUCO resulted from the symmetry-allowed interaction between the LUCO of the polyacetylene skeleton and the p_z orbitals of the sulfur atoms.[52] The LUCO was destabilized in energy by this antibonding interaction.

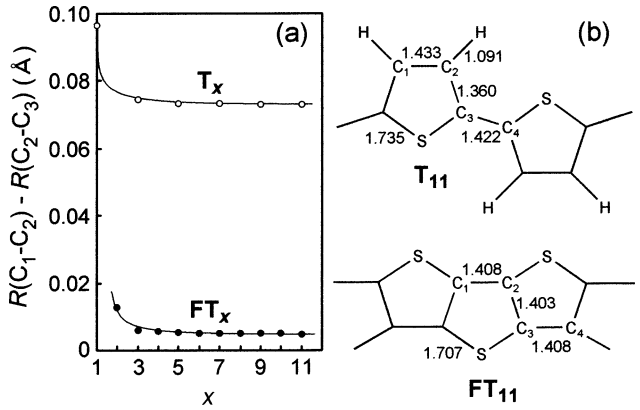

Figure 1. Bond alternation for oligothiophenes ($\mathbf{T}_x$) and fused oligothiophenes ($\mathbf{FT}_x$) concerning their central moieties (a) and optimized structures of the 11-mers (b). Bond lengths are in Å.

The band gap values corresponded to the direct transition at $k = 0$ because in both polymers the HO band was highest and the LU band was lowest at $k = 0$ as shown in Figure 2. The PM5 calculated band structure of **PT** was very similar to those from VEH calculations by Brédas et al.[41] and ab initio calculations by André et al.[51] The PM5 calculated band gap for **PT** was 6.45 eV. In comparison with the absolute value of the experimental band gap for **PT** (E_g^{exp} = 2.1 eV),[40] the PM5 SCF value was higher by 4.35 eV due mainly to the neglect of the electron correlation effects. The PM5-calculated band gap for **LPT** was 5.92 eV which was smaller than that of **PT** by 0.53 eV. It has been suggested that, for many polymers, the correlation effects result only in an almost constant shift of the electronic levels.[36] According to this assumption, one could roughly approximate a more reliable band gap of 1.5−1.6 eV for **LPT**.

As shown in Figure 2, the nodal pattern of the HOCO was characteristic of the benzenoid form while that of the LUCO was characteristic of the quinonoid form. The decrease in band gap for **LPT** relative to **PT** can be attributed to an increase in the quinonoid contribution to the electronic structure, which destabilized the HOCO and stabilized the LUCO. However, the contribution from the quinonoid structure in **LPT** was partly canceled out by the remarkable antibonding interaction with twice as many sulfur p_z orbitals as those in **PT** to destabilize the LUCO in energy. As a result, the band gap for **LPT** was not so small as that predicted from the almost vanished bond length alternation ($\delta r = 0.005$ Å).[9]

4.2. Optimized Structures of Charged Defects. We show in Figure 3 the PM5-optimized structures of $\mathbf{FT_2}$, $\mathbf{FT_2}^+$ (cation radical), and $\mathbf{FT_2}^{2+}$ (dication), together with illustrations that characterize the behavior of the optimized C−C bond lengths. While the outermost

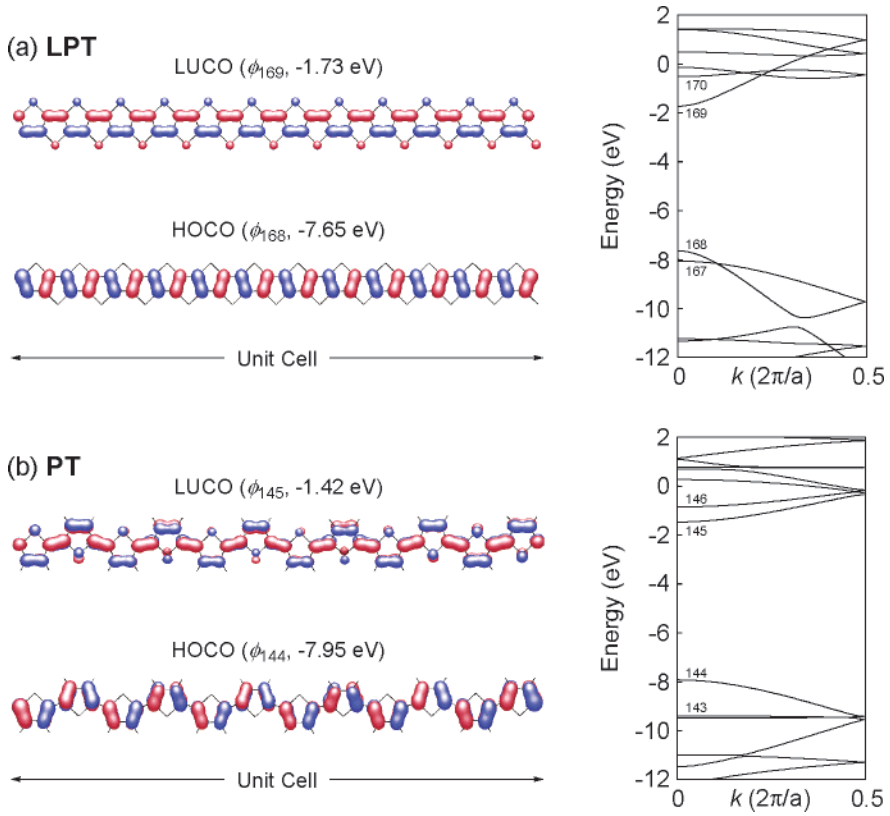

Figure 2. PM5-calculated crystal orbitals in the frontier orbital region and band electronic structures for (a) **LPT** and (b) **PT**.

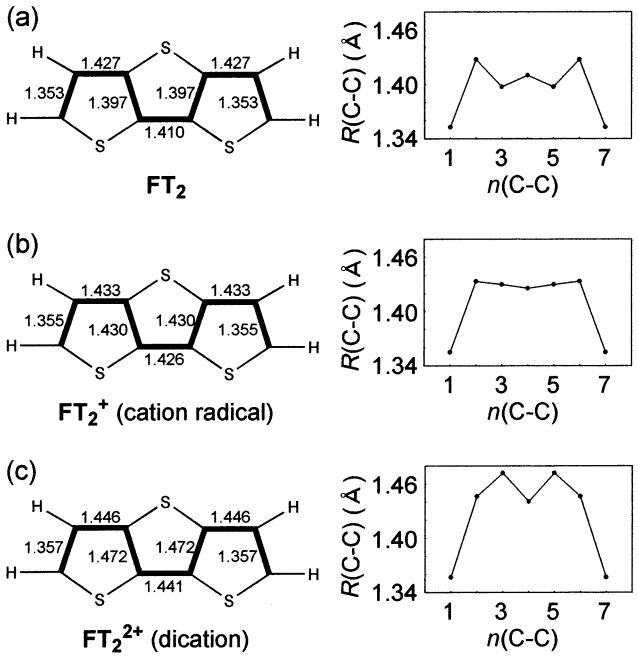

Figure 3. Structures of (a) $\mathbf{FT_2}$, (b) $\mathbf{FT_2}^+$, and (c) $\mathbf{FT_2}^{2+}$ as obtained at the PM5 level and the trends in the behavior of the C−C bond lengths along the conjugated π system.

$C_\alpha-C_\beta$ and $C_\beta-C_\beta$ bonds (i.e., n(C−C) = 1, 2, 6, and 7) in these molecules represented clear benzenoid edges due to the chain-end effects, the C−C bonds in the middle of the molecules (i.e., n(C−C) = 3, 4, and 5) were characterized by the alternation pattern which changed according to the oxidation state. A weak benzenoid-type pattern was observed for the conjugated π system of neutral $\mathbf{FT_2}$ with the degree of alternation much smaller than that of oligothiophene,[42] which was consistent with the results in Figure 1. On the other hand, a reversed quinonoid-type pattern was weakly observed for singly charged $\mathbf{FT_2}^+$, and it was enhanced in doubly charged $\mathbf{FT_2}^{2+}$. However, the number of C−C bonds in $\mathbf{FT_2}^{n+}$ were too small to eliminate the effect of benzenoid edges which overshadowed the structural properties of the chain.

With increasing chain length, we could observe systematic trends in the evolution of the structures of charged defects. The structure characteristic of the rings in neutral $\mathbf{FT}_x$ gradually developed when the benzenoid edges were far apart, as shown in the left column of Figure 4a. The typical geometry modifications appearing upon formation of a positive polaron are shown in the center column of Figure 4a. The C−C bonds lengths characteristic of the rings at the center of the semiquinonoid defect were already present in $\mathbf{FT_3}^+$. As the chain elongated, the amplitude of the geometric changes was found to diminish progressively when going from the center to the end of the molecule. The structure characteristic of the neutral rings appeared as the transition regions between the semiquinonoid center and the benzenoid edges in $\mathbf{FT_9}^+$, though it extended only over the outermost ring for the oligomer sizes considered here. Comparison of the C−C bond lengths of $\mathbf{FT_7}^+$ and $\mathbf{FT_9}^+$ demonstrated that for n(C−C) = 24 (i.e., 6 fused rings) the structure characteristic of the polaronic defect converged. The C−C lengths of molecules in the singly oxidized state were intermediate between the values obtained in the neutral and doubly oxidized states and thus showed the appearance of a semiquinonoidal character along the chain. On the other hand, the region with a bipolaronic quinonoid structure in $\mathbf{FT_9}^{2+}$ extended over the whole molecule except for the benzenoid edges, as shown in the right column of Figure 4a. The transition regions between benzenoid

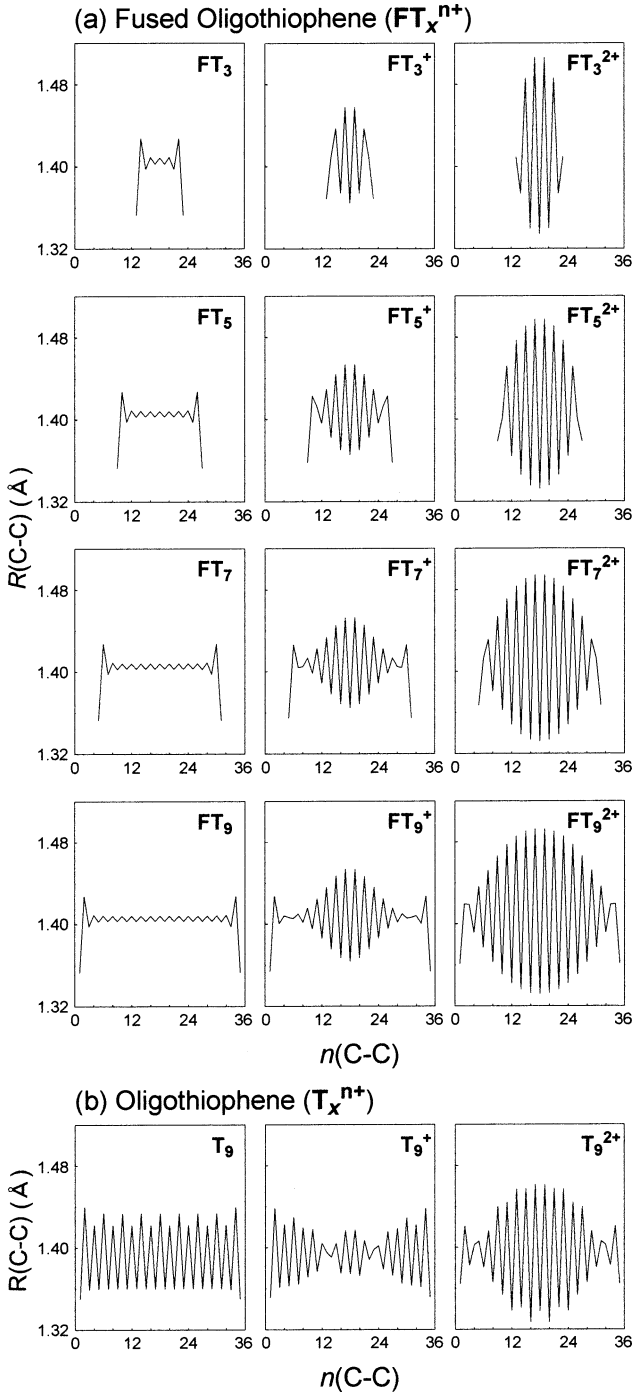

Figure 4. PM5-optimized C−C bond length in Å for (a) the fused oligothiophenes ($\mathbf{FT}_x^{n+}$, x = 3, 5, 7, 9) and (b) nonathiophene ($\mathbf{T}_x^{n+}$, $x = 9$) in the neutral ($n = 0$), singly oxidized ($n = 1$), and doubly oxidized ($n = 2$) states. Bonds with the smallest and the largest number lie at the end of the chain. See Figure 3 for $x = 2$.

edge regimes and the quinonoid center were not yet structurally converged for n(C−C) = 30 in $\mathbf{FT_9}^{2+}$. The optimized geometry of the dication exhibited a large width of structural modifications up to 44 C−C bonds on the fused rings, as discussed later.

We show in Figure 4b the evolution of charged defect structures from nonathiophene (**T₉**). With the exception of small subtleties, the overall picture of the PM5-optimized structural modifications in $\mathbf{T_9}^{n+}$ (n = 1 or 2) were essentially identical with those from ab initio 3-21G* and PM3 calculations[42] and from AM1 calculations.[43] Comparison of the structures of $\mathbf{FT_9}^{n+}$ and $\mathbf{T_9}^{n+}$ in Figure 4 revealed that both polaronic and bipolaronic regions were structurally more distinct and extended in $\mathbf{FT_9}^{n+}$. This indicated that transformation to the quinonoid forms during the geometry relaxation process was much easier from the fused rings in **FT₉** with almost vanished bond alternation, than from the thiophene rings in **T₉** with a clear benzenoid-type character.

The optimized geometry of the singly and doubly oxidized unit cells were consistent with the formation of positive polaron and bipolaron, as mentioned earlier. We calculated the structure of sufficiently large unit cells containing 48 carbon atoms (i.e., n(C−C) = 47) for **LPT** and **PT** to accommodate +1 charge per unit cell, taking into account the calculated width of polaronic regions in the oligomers. We show in Figure 5 the optimized structures of two adjacent unit cells for **LPT** and **PT**. The charged defects in these polymers were located across the cell boundary, and were characterized by a reversal of the single-double C−C bond pattern; the geometry relaxation process thus induced the appearance of a strong quinonoidic character within the unit cell. The behavior of the C−C bonds shown in Figure 5 was qualitatively very similar to the corresponding data for oligomers in Figure 4. Essentially, all the trends in the case of polymers were also present in oligomers except for the benzenoid edges. For a unit cell of this size, the bipolaronic defect and the transition regions in **LPT** can definitely be considered as having sufficiently converged. We estimated that an upper limit for the width of the bipolaronic geometry relaxation for **LPT** corresponded to a length of n(C−C) = 44 (11 thiophene rings). The widths of charged defects in **LPT** and **PT** were almost identical with those in the corresponding oligomers, or slightly larger by three to four C−C bonds due to the absence of chain-end effects.

The question of whether the polaron or the bipolaron is the lowest-energy charge storage configuration is of fundamental importance. Although the self-consistently generated structural distortions in the doubly oxidized state lead to the bipolaron as the lowest energy configuration, Coulomb repulsion should favor two separated polarons. Thus, depending on the relative strength of electron−phonon and electron−electron interactions, the polaron creation energy (E_p) and the bipolaron creation energy (E_b) could be comparable.[6] For weak electron−electron repulsion, $E_b < 2E_p$ so that two polarons would couple to give a bipolaron, while in the case of strong Coulombic interactions, $E_b > 2E_p$ so that the two separate polarons would be favored over a bipolaron. We show in Figure 6 energetic aspects of doping behaviors for **LPT** and **PT**, predicted by PM5 calculations. As mentioned earlier, the polaron−polaron coupling within a chain was forbidden by the translational symmetry imposed on the polymer models in the present treatment. However, we can predict from the following considerations whether polaron or bipolaron is energetically favored. Consider two unit cells containing x carbon atoms (C_1, ..., C_x) and $2x$ carbon atoms (C_1, ..., C_{2x}), respectively, as shown in Figure 6. A polaron state with a doping level of $y_C = +1/x$ is generated by allocating a +1 charge to the former cell, while a bipolaron state at the same doping level is represented by the latter cell accommodating a +2 charge. A set of two unit cells in the polaron model contains $2x$ carbons (C_1, ⋯ C_x, C_{x+1}, ⋯ C_{2x}) and +2 charge, and is not

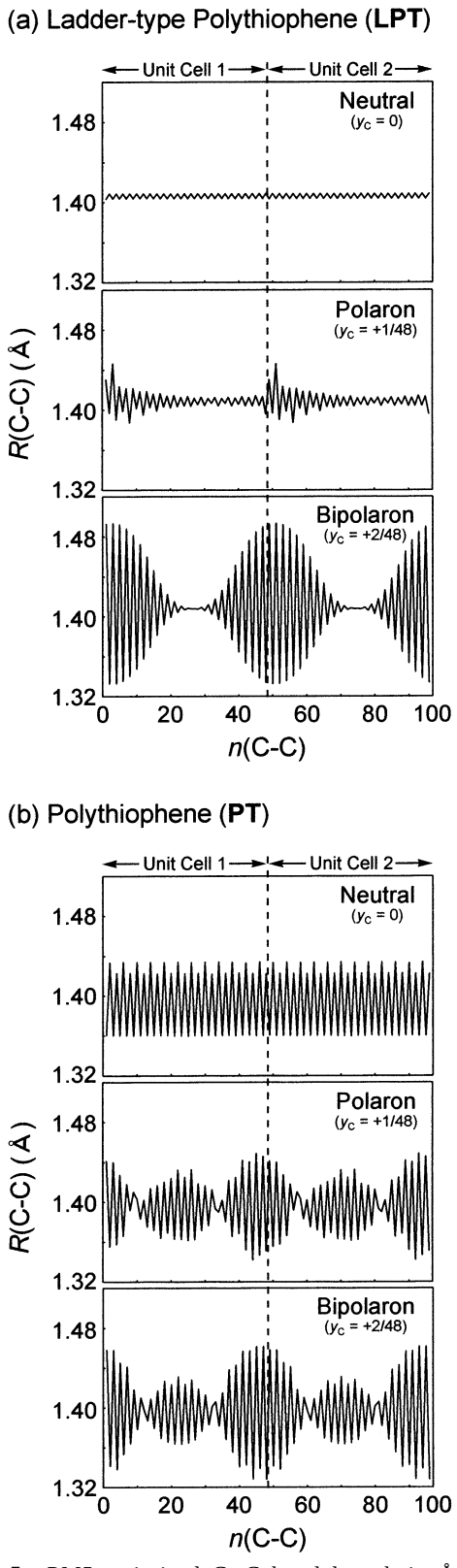

Figure 5. PM5-optimized C−C bond length in Å for two adjacent unit cells of (a) **LPT** and (b) **PT** in the neutral, polaron, and bipolaron states. The unit cell contained 48 carbon atoms. Charges of +1 and +2 were allocated to the unit cells to represent the polaron state (y_C = +1/48) and the bipolaron state (y_C = +2/48), respectively.

different from the single unit cell of the bipolaron model except the nature of the charge storage configuration. An energy change associated with the transition from two polarons into a bipolaron without the change in y_C can be approximated from

$$\Delta H_f = H_f^{cell(b)}/N_C^{cell(b)} - H_f^{cell(p)}/N_C^{cell(p)} \quad (1)$$

where $H_f^{cell(b)}$ and $H_f^{cell(p)}$ are the heat of formation calculated for single unit cells of the bipolaron and polaron models, respectively, and $N_C^{cell(b)}$ and $N_C^{cell(p)}$ are the numbers of carbon atoms in the cell (i.e., $N_C^{cell(b)} = 2x$ and $N_C^{cell(p)} = x$ for the bipolaron and polaron models, respectively). The charge storage configurations is determined not only by doping levels but also by the dielectric constants of the medium and interchain interactions, because they can affect the Coulombic interaction between the charged localized states to change the relative stability of polarons and bipolarons. In the present study, however, we calculated the energies of isolated macromolecules without any consideration of the medium effect, and restricted the discussion to the qualitative trends in the relative stability of charged species.

We show in Figure 6 how H_f^{cell}/N_C^{cell} changed in **LPT** and **PT**, according to y_C. In **PT**, the bipolaron was the lower-energy state than the polaron ($\Delta H_f < 0$), as shown in Figure 6b. The normalized energy change calculated for the polaron−polaron coupling in **PT** at a doping level of $y_C = +1/24$, for example, was $\Delta H_f = -0.87$ kcal/N_C^{cell}. This result was consistent with the experimental evidence in the case of **PT** and poly(3-methylthiophene) that, upon oxidative doping, a charge was stored in spinless bipolarons though polarons were also generated by very dilute dopings.[6] The existence of polarons at very low concentrations going over to bipolarons at higher concentrations suggested that the reaction of two polarons into a bipolaron was inhibited at very low concentrations. Indeed, Figure 6b tells us that the driving force for the polaron−polaron coupling (i.e., $-\Delta H_f$) is decreased as y_C is lowered, and that it could eventually be small enough to allow persistence of polarons at very low y_C. In this context, injection of a single charge must always occur via the formation of polarons, with bipolarons resulting from the reaction of two polarons.

In **LPT**, however, the coupling of polarons was uphill in energy ($\Delta H_f > 0$), as shown in Figure 6a. The polarons turned out to be the prevailing charged species even at fairly heavy doping regimes. At a doping level of $y_C = +1/24$, for example, the polaron was favored over the bipolaron by $\Delta H_f = 0.62$ kcal/N_C^{cell}. The energy difference was essentially unaffected by y_C. The formation of a paramagnetic charged carrier was experimentally supported by the ESR spectrum of the doped **LPT**, as mentioned later.

4.3. Synthesis. The oligomers were synthesized by the superacid-induced condensation of thenyl sulfoxides, according to Scheme 1. The synthesis and characterization of $\mathbf{FT}_x$ by this method was, however, predicted to be difficult because of the side reaction at terminal positions during the condensation process. To block the reactive termini, methyl groups were introduced as the end group to the oligomers ($\mathbf{Me_2FT}_x$, $x = 2, 3$) in Scheme 1. The decylsulfanyl-substitued bithiophene (**DS-T$_2$**) and terthiophene (**DS-T$_3$**) having terminal methyl groups were prepared by the Suzuki aryl−aryl coupling reaction followed by the Vilsmeier formylation and the reduction of the resulting aldehyde (see Supporting Information). The decylsulfanyl group was selected as the pendant group, to achieve sufficient solubility after ring closure.

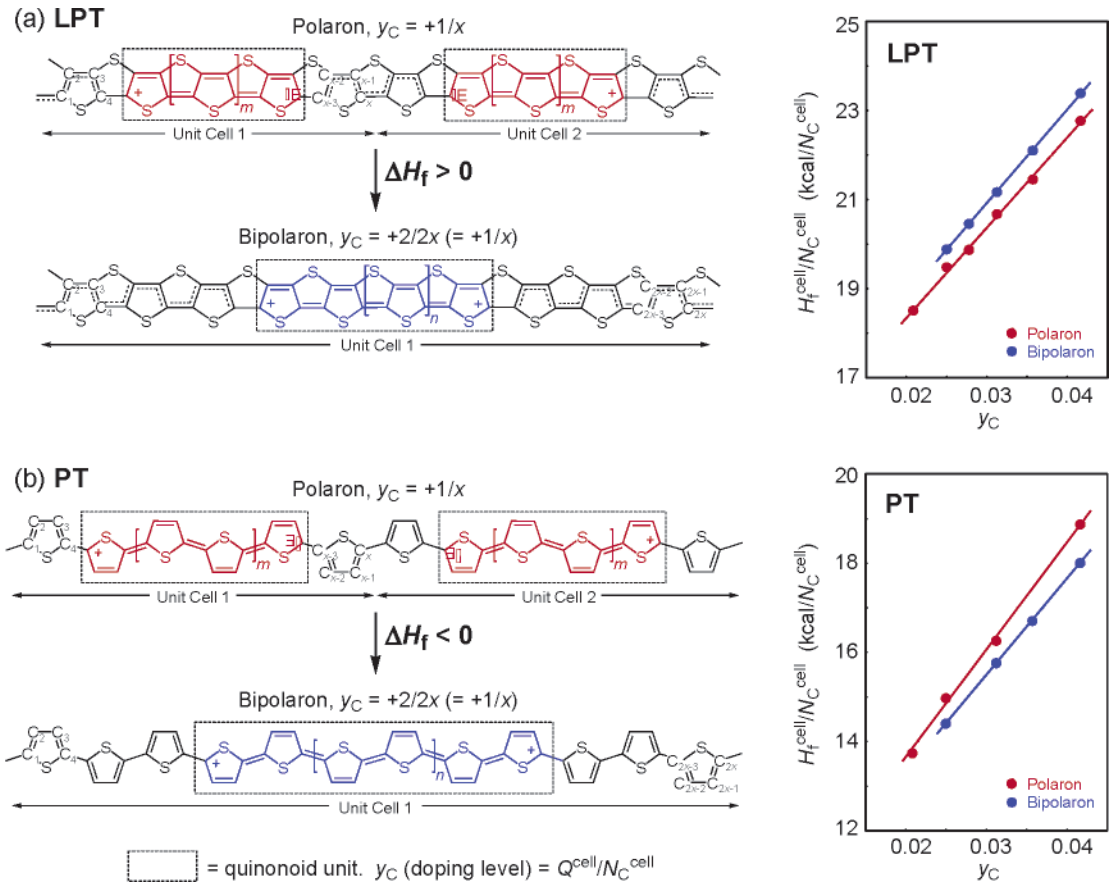

Figure 6. Schematic diagram for the reaction of two polarons into a bipolaron along the chain in (a) **LPT** and (b) **PT** and heat of formation calculated for the polaron and bipolaron states at various y_C. The polaron model was a singly oxidized unit cell ($Q^{cell(p)} = +1$) containing x carbon atoms ($N_C^{cell(p)} = x$), and the bipolaron model was a doubly oxidized unit cell ($Q^{cell(b)} = +2$) containing $2x$ carbon atoms ($N_C^{cell(b)} = 2x$). The doping levels for the two models were thus equalized at $y_C = Q^{cell}/N_C^{cell} = +1/x$. A pair of polarons were represented by a set of two adjacent unit cells, which was isostructural to the single cell of the bipolaron model except the configuration of charge storage. The normalized heat of formation (H_f^{cell}/N_C^{cell}) was calculated for a single unit cell and expressed in units per N_C^{cell}.

The decylsulfanyl group in **DS-T$_x$** was successfully converted to a decane-1-sulfinyl group by the treatment with peracetic acid at room temperature to yield **DSO-T$_x$** (Scheme 1). The reaction was not accompanied by the further oxidation to a decane-1-sulfonyl group, which was confirmed by the absence of IR and NMR signals attributed to sulfones (ν_{SO2} = ca. 1150 and 1350 cm^{-1}) in the product. The ring closure of **DSO-T$_x$** to give fused oligothiophenes (**D-Me$_2$FT$_x$**) was accomplished by the intramolecular condensation of the sulfoxide in triflic acid, which proceeded essentially to completion. In this reaction, the protonated sulfoxide (i.e., the hydroxysulfonium ion) electrophilically attacked the adjacent thiophene ring to form a λ^4-decylsulfanyliumdiyl linkage that forced the two thiophene rings into planarity. The ring-closing reaction did not proceed at room temperature and required heating at 80 °C. Triflic acid, the strongest monobasic acid, was found to be most effective for the reaction. The byproducts from intermolecular condensation were not formed, when the reaction was carried out under the diluted conditions. In NMR, the methylene unit adjacent to the sulfur atom of the λ^4-decylsulfanyliumdiyl group in **D-Me$_2$FT$_x$** was more deshielded than that of the decane-1-sulfinyl group in **DSO-T$_x$**, as a result of the enhanced electron-withdrawing effect of the sulfonium ion relative to the sulfoxide. The NMR peaks in the aromatic region (^{1}H, singlet; ^{13}C, four peaks) were indicative of the C_{2v} symmetric structures of **D-Me$_2$FT$_x$**. IR spectra of **D-Me$_2$FT$_x$** showed characteristic bands of the triflate anion. The dealkylation of the λ^4-decylsulfanyliumdiyl group was accomplished by the treatment with refluxing pyridine to give **Me$_2$FT$_x$** (x = 2, 3) (Scheme 1). The absence of the decyl group and the triflate anion in **Me$_2$FT$_x$** were confirmed by spectroscopic methods (see Experimental Section).

Regioregular (head-to-tail) polythiophenes 3-substituted with alkylsulfanyl groups have been synthesized by several methods.[53−55] In the present study, **DS-PT** (M_n = 5800, M_w/M_n = 1.2) was prepared by McCullough's Grignard coupling method,[46−48] and **MS-PT** (M_n = 5000, M_w/M_n = 1.5) was prepared by the Stille coupling method using thienyl stannane (see Supporting Information). The HT-HT regioregularity of **DS-PT** and **MS-PT** were 97% and 95%, respectively, which were determined from the ^{1}H NMR spectra.

The alkylsulfanyl groups in **DS-PT** and **MS-PT** were quantitatively oxidized by peracetic acid to the corresponding alkane-1-sulfinyl groups in **DSO-PT** and **MSO-PT**, respectively (Scheme 2). Undesired alkane-1-sulfonyl groups were not found in the oxidized products. GPC analyses revealed that no molecular-weight degradation occurred during the oxidation. The polymer-analogous ring-closing reaction was accomplished by the treatment with triflic acid at 80 °C to give **D-LPT** and **M-LPT** from **DSO-PT** and **MSO-PT**, respectively. The ring-closed products were soluble in DMSO and $CHCl_3$, and were fully characterized by spectroscopy. The

Scheme 1. Synthesis of Fused Oligothiophenes (Me_2FT_x)

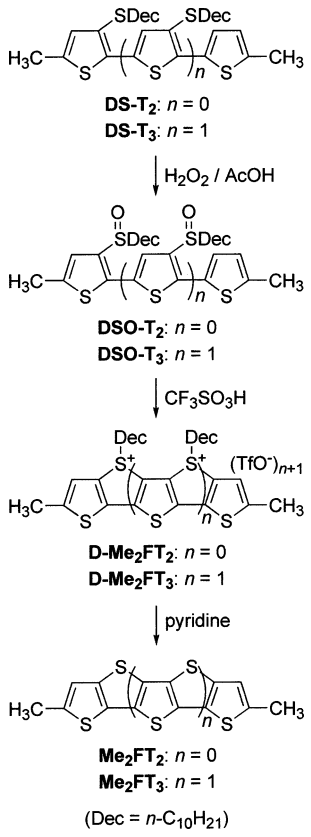

Scheme 2. Synthesis of Ladder-type Polythiophene (LPT)

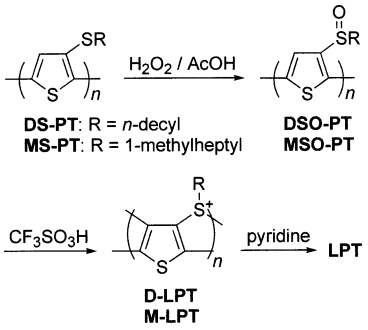

resonance of methylene groups adjacent to the sulfur atom in **DSO-PT**, for example, showed a downfield shift upon the ring closure, which was consistent with the spectral changes encountered in the case of **DSO-T_x**. There was no remaining decane-1-sulfinyl resonance in the ^{1}H NMR spectrum of the product (Figure S1). The IR and NMR spectra indicated that intermolecular λ^4-alkylsulfanyliumdiyl linkages were unlikely formed in **D-LPT** and **M-LPT**. No structural defect in **D-LPT** or **M-LPT** was visible in the spectra, although they should contain at least 3−5% of defects according to the regioregularity of the corresponding prepolymers.

The ladder-type polythiophene (**LPT**) was prepared from **D-LPT** by the dealkylation of the λ^4-decylsulfanyliumdiyl group; **LPT** was obtained as an insoluble and infusible dark red powder. A thin film of **LPT** on a glassy carbon electrode for electrochemical characterization was prepared by the spin coating of **M-LPT** from the $CHCl_3$ solution followed by the conversion to **LPT** in situ by the dealkylation of the λ^4-(1-methyl)heptylsulfanyliumdiyl group in **M-LPT**.

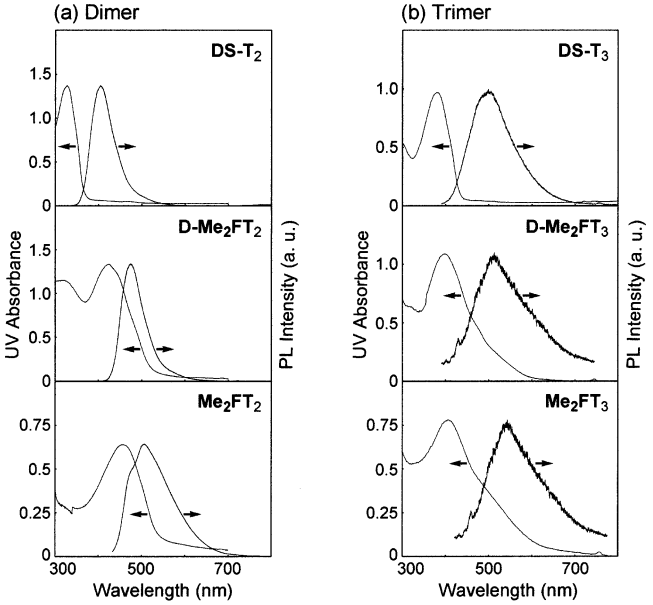

Figure 7. UV−vis absorption spectra and photoluminescence spectra (excited at $\lambda_{max\ abs}$) of (a) the dimers (0.1 mmol/L in $CHCl_3$) and (b) the trimers (0.02 mmol/L in CH_3CN). The optical path length was 1 cm.

4.4. Spectroscopic and Electrochemical Properties. We show in Figure 7 the UV−vis absorption and photoluminescence spectra of the oligomers in solution. The ring closure (**DS-T_x** → **D-Me_2FT_x**) and the conversion to fused oligothiophenes (**D-Me_2FT_x** → **Me_2FT_x**) induced the shift of the absorption maxima ($\lambda_{max\ abs}$) and the emission maxima ($\lambda_{max\ em}$) to longer wavelengths. For the three series, i.e., **DS-T_x**, **D-Me_2FT_x**, and **Me_2FT_x**, the luminescence spectra shifted to lower energies with the increase in the length of the oligothiophene segments. Similar trends were also observed for the absorption spectra except the **Me_2FT_x** series: the $\lambda_{max\ abs}$ of **Me_2FT_3** was blue-shifted by 50 nm compared to that of **Me_2FT_2**, while **Me_2FT_3** displayed a pronounced tailing of the longest wavelength absorption band into the low energy region (i.e., occurrence of a low-energy absorption shoulder). These absorption and emission behaviors may be related to the longer conjugation length along the fused oligothiophenes responding in lower $\pi-\pi^*$ transition energies, although a steep absorption edge and well-resolved vibronic fine structure is characteristic of planar one-dimensional π-systems. At any rate, the reduction of the HOMO−LUMO gap expected for the fused ring structures was supported by the lower $\pi-\pi^*$ transition energies for **Me_2FT_x**. Part of the red shift in the absorption spectra may also be coupled to the contribution from the inductive effect of the sulfur atom. However, no definitive conclusions in this regard can be derived from the spectra.

The absorption and emission spectra of the polymers in $CHCl_3$ are displayed in Figure 8. The lower solubility of **D-LPT** than others was reflected in the lower absorbance and emission intensities. The spectra of **DS-PT** and **D-LPT** were similar to those of **MS-PT** and **M-LPT**, respectively. Comparison between poly(3-alkylsulfanylthiophene)s and the ring-closed products revealed that the latter exhibited much longer wavelengths of absorption and luminescence. In particular, **M-LPT** showed a very wide absorption band with weak vibronic structures whose cutoff was located at 795 nm, and a smaller Stokes loss of $\Delta\lambda$ = 63 nm between

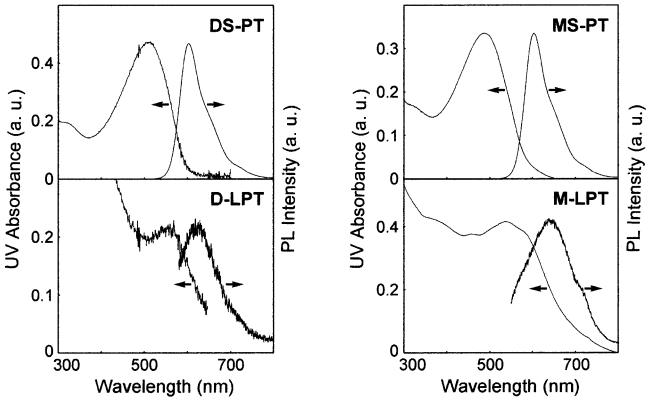

Figure 8. UV−vis absorption spectra and photoluminescence spectra (excited at $\lambda_{\max abs}$) of poly(3-alkylsulfanylthiophene) (ca. 0.1 mmol unit/L) in $CHCl_3$, and the corresponding ring closed polymers in saturated $CHCl_3$ solutions. The alkyl groups were (left) the decyl group and (right) the 1-methylheptyl group.

$\lambda_{\max abs}$ and $\lambda_{\max em}$ than **MS-PT** ($\Delta\lambda$ = 118 nm), as a consequence of the geometrically fixed ladder structure that allows minimum changes of the polymer geometry during the $\pi-\pi^*$ transition. These results suggested that the π-electrons in the ring-closed polymers delocalized along the chain to extend the degree of conjugation. In contrast, the main chain of **DS-PT** and **MS-PT** were more twisted due to the attached alkylsulfanyl side chains, which reduced the conjugation length of the main chain. The small absorption tails for **D-LPT** and **M-LPT** between 650 and 750 nm were caused by the very low concentration of the sample solutions. Unfortunately, the spectrum of **LPT** was not obtained because **LPT** did not form a transparent film on a glass substrate. A thin film of **LPT** was, instead, formed on a glassy carbon electrode and electrochemically characterized, as described below.

We show in Figure 9a cyclic voltammograms recorded for solutions of the dimers in CH_3CN in the presence of $TBABF_4$ as the supporting electrolyte. The voltammogram for **DS-T$_2$** showed an oxidation peak at 1.13 V which was assignable to the oxidation of the sulfide.[56,57] The unresolved oxidation wave for **D-Me$_2$FT$_2$** appeared near 1.2 V. When the potential was scanned in a negative direction, no reduction occurred for **DS-T$_2$** and **D-Me$_2$FT$_2$** before −1.3 V except the rereduction of the oxidized products. On the other hand, a quasi-reversible reduction−oxidation peak couple was observed for **Me$_2$FT$_2$** at −0.72 V. The reduction of **Me$_2$FT$_2$** corresponded to the formation of a stable anion radical by one-electron reduction, which was related to the n-doping process in the case of the polymer. The reduction potential of **Me$_2$FT$_2$** was much more positive than that of **DS-T$_2$** due to the higher electron affinity of the fused rings, which suggested that **LPT** would more readily undergo n-doping than **PT**.

The redox behavior of **DS-PT**, **D-LPT** and **LPT** as coated films on a glassy carbon electrode was studied by cyclic voltammetry. All of these polymers displayed the first oxidation peaks at $E_p^+ \approx 1.0-1.4$ V which were assignable to the p-doping process, as shown in Figure 9b. The unresolved rereduction wave appeared near $E_p^- \approx 0.9$ V for **DS-PT** assignable to the dedoping process, while those for **D-LPT** and **LPT** were overshadowed by the broad reduction peaks near −0.3 V. The second oxidation peak at 1.2 V for **DS-PT** was assigned to the oxidation of the decylsulfanyl group in the polymer.[56]

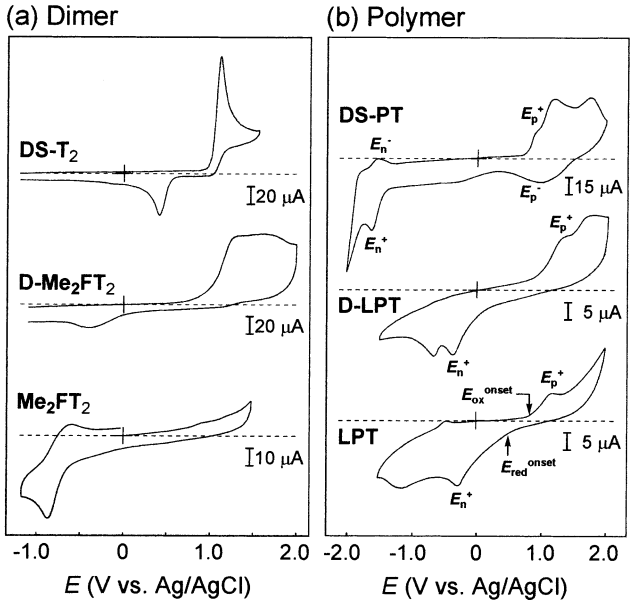

Figure 9. Cyclic voltammograms of (a) the dimers as 1 mmol/L solutions and (b) the polymers as films coated on a working electrode, recorded in CH_3CN containing 0.1 mol/L $TBABF_4$. Scan rate: 50 mV/s. The films of **DS-PT** and **D-LPT** were prepared by spin coating from $CHCl_3$ solutions. The **LPT** film was prepared from the **D-LPT** film by dealkylation in situ (see Experimental Section).

On sweeping negatively, **DS-PT** showed a reduction peak at $E_n^+ = -1.6$ V and a reoxidation peak at $E_n^- = -1.5$ V, which were assignable to the n-doping and dedoping processes, respectively. The reduction peaks assignable to the n-doping process for **D-LPT** and **LPT** appeared at $E_n^+ = -0.4$ V and −0.3 V, respectively. The second reduction peak at −0.7 V for **D-LPT** was assigned to the reduction of the sulfonium ion.[56] Repeated cycling of these polymers in the p- and n-doping regions showed almost no loss of charge capacity.

Cyclic voltammograms of **D-LPT** and **LPT** showed broad redox waves for the n-doping cycle but clearly illustrated the low band gap nature of these polymers. Estimation of the band gaps from the p-doping (E_p^+) and n-doping (E_n^+) peak potentials yielded approximate values of 2.5 eV for **DS-PT**, 1.8 eV for **D-LPT** and 1.5 eV for **LPT**. The electrochemically determined band gaps were not necessarily reliable values because of the difficulty in electrochemical doping which could lead to large overpotentials and broad redox waves. In particular, the oxidation and reduction onset potentials for **LPT** as measured for the p- and n-doping processes were $E_{ox}^{onset} \approx 0.9$ V and $E_{red}^{onset} \approx 0.5$ V, respectively, which corresponded to a band gap of ca. 0.4 eV, much smaller than derived from the peak potentials. However, observed qualitative trends were consistent with the reduction of the band gap induced by the fused ring structure. The band gap decrease came mainly from the positive shift of E_n^+ for **D-LPT** and **LPT**. An estimation of the LUMO energy from E_n^+ was possible by correlation with the vacuum energy of the ferrocene/ferrocenium standard (−4.8 eV).[58,59] For **LPT**, this calculation resulted in a value of −3.1 eV for the LUMO level. This energy level was much lower than the LUMO levels of conventional electron transport materials in light-emitting diodes, such as 2-(4-biphenyl)-5-(4-*tert*-butylphenyl)-1,3,4-oxadiazole (−2.4 eV),[60] and may provide a closer match to the work function of the magnesium cathode (−3.7 eV)[61] in LEDs.

Table 1. Doping Levels and Electric Conductivities of I_2-Doped Polymers

polymer	iodine/polymer[a] (wt %)	$10^2 y_C$[b]	σ_{RT} (S/cm)[c] pellet[d]	film[e]	ref
PT	71	2.3 (43)	2.3		62
	47	1.5 (67)	4.0		this work
H-PT				600	63
	40	2.6 (38)	3.0	300	this work
M-LPT	7.5	1.1 (91)	0.003	1	this work
LPT	52	2.3 (43)	0.6	300	this work

[a] Doping was conducted by exposing a powder or a film to a vapor of iodine at 10 mmHg for 24 h. The excess iodine was removed under vacuum, and the amount of iodine taken into the polymer was determined by weighing. [b] Mean charge per number of carbon atoms on a chain calculated from the iodine content, assuming that the dopant was I_5^- according to ref 62. For example, when 1 g of pristine **PT** was doped with 0.71 g of I_5^- (iodine/polymer = 71 wt %), the carbon atoms in **PT** were $N_C = 4/88$ mol and I_5^- ions (=positive charges on **PT**) were $Q = 0.71/(127 \times 5)$ mol. The doping level (y_C) was obtained from $y_C = Q/N_C$ to be 0.023. Mean numbers of carbon atoms per charge ($1/y_C$) are shown in parentheses. [c] Electric conductivities at room temperature determined by four-probe methods. [d] Pressed pellets obtained from doped powder samples. [e] Polymer films cast from $CHCl_3$ solutions. The doping levels were not determined for film samples. The values of σ_{RT} are averages for five samples varying film thicknesses, which ranged from 10 to 50 μm.

4.5. Characterization of the p-Doped States. The doping was carried out by the exposure of powdery samples or films to I_2 vapor for a sufficiently long time to ensure saturation of the doping level. The doping level (y_C) was determined by the gravimetric analysis of the doped sample, assuming that the dopant was I_5^- and that the doping reaction went to completion with each I_5^- ion yielding a transfer of one electron from the polymer chain.[62] The iodine contents and the calculated values of y_C for the I_2-doped **M-LPT** and **LPT** are listed in Table 1, together with those of **PT**[62] and poly(3-hexylthiophene) (**H-PT**)[63] as the standard samples. These polymers showed almost the same level of doping at saturation ($y_C = 0.02-0.03$) except **M-LPT**. The lower y_C for **M-LPT** was the result of the positive charges on the sulfonium ion which suppressed further positive charging by the oxidative doping. The I_2-doped **LPT** exhibited electric conductivities of approximately 10^0 S/cm for the pellet sample and 10^2 S/cm for the film, which were determined by the four-probe method at room temperature. Despite the smaller band gap for **LPT**, the dopant concentration and the conductivity of **LPT** were comparable to those of **PT** and **H-PT**.

On the other hand, the charge storage configuration in **LPT** was quite different from that in **H-PT**. We show in Figure 10a the ESR signals obtained with the I_2-doped powder samples of **M-LPT** and **LPT**, which revealed the significant formation of paramagnetic charge carriers (polarons). Considering that the doping levels were relatively high, this charge storage configuration was quite unusual for conducting polymers.[6] In the case of poly(3-methylthiophene), for example, it was reported that the charge was stored in spinless bipolarons in the solid state, with the presence of a maximum of ca. 0.2 mol % polarons (one spin per 500 rings) at low doping levels.[64] The I_2-doped **H-PT** likewise carried only a trace amount of spin and exhibited a very weak ESR signal as shown in Figure 10b. The spin concentrations for I_2-doped **M-LPT** and **LPT** were roughly estimated from the doubly integrated intensities of the ESR signals relative to that of a 2,2,6,6-tetramethyl-1-piperidinyloxy (TEMPO) solution as a standard. The spin concentrations were approximately on the orders of 10^{19} spin/g for **M-LPT** and 10^{20} spin/g for **LPT**, and their correlation to the doping levels revealed that major parts of the positive charges existed as polarons. These results were consistent with the relative stability of the polaron and bipolaron states in **LPT** which was reversed from that in **PT**, according to the PM5 calculations in Figure 6. The ESR spectra consisted of a single line at $g = 2.0035$ for **D-LPT** and 2.0037 for **LPT**. These g-factors were higher than the values commonly observed for p-doped π-conjugated polymers[65] and oligomers,[66] such as the cation radical of didodecylsexithiophene ($g = 2.0023$) which corresponded to a (nearly) free radical.[67] Unusually high g-factors were reported for p-doped poly(dithienothiophene)s ($g \approx 2.004$) which originated from the strong spin−orbit coupling within the polymer containing the fused moieties.[24] The high g-factors for doped **D-LPT** and **LPT** were assumed to be characteristic of a similar fused ring structure, which suggested that the sulfur atoms were substantially involved in the SOMOs. Because the polaron was the lowest-energy charge storage configuration, the p-doped **M-LPT** and **LPT** were stable polyradicals maintaining the spin concentration at room temperature.

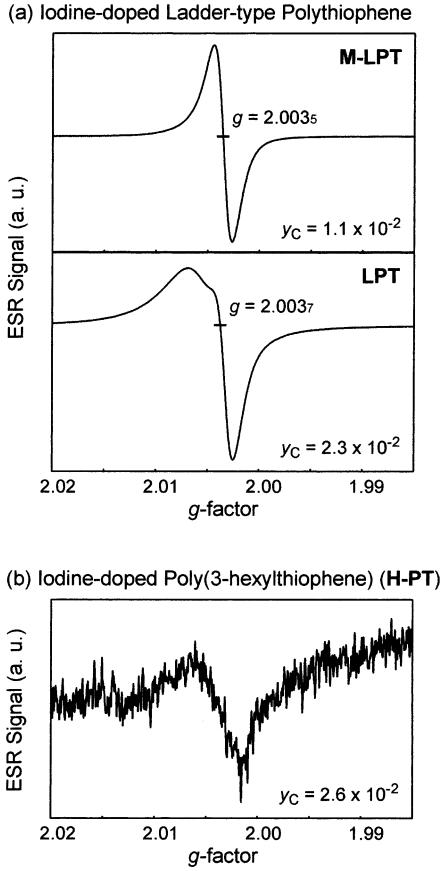

Figure 10. Solid-state ESR spectra of p-doped (a) **M-LPT** ($y_C \approx +1/91$), **LPT** ($y_C \approx +1/43$), and (b) **H-PT** ($y_C \approx +1/38$) at the saturated levels of doping achieved by the exposure of powdery samples to I_2 vapor at 10 mmHg for a sufficiently long time (ca. 24 h). The doping level (y_C) was defined as the amount of charge per number of carbons, which was determined by the gravimetric analysis of the doped sample, assuming that the dopant is I_5^-. Spectra were arbitrary rescaled.

5. Conclusions

A novel π-conjugated ladder-type polymer composed of fused thiophene rings was synthesized and characterized. Band electronic structures were discussed in view of geometrical changes imposed by the fused ring structure. The reduction of the band gap from that of polythiophene was attributed to an increase in the quinonoid contribution to the electronic structure, which destabilized the HOMO and stabilized the LUMO. The smaller HOMO−LUMO gap was experimentally supported by the lower $\pi-\pi^*$ transition energies and the smaller gap between electrochemical p- and n-doping potentials. The structures of charged defects emerged from the systematic investigation of the equilibrium structures of oligomer models in their singly and doubly oxidized states. At the center of these defects, the originally benzenoid structure changed to a quinonoid structure, thereby reversing single and double bonds. The spatial extension of the polaronic defect amounted to 24 C−C bonds, while the bipolaronic defect extended over 44 C−C bonds. Both polaronic and bipolaronic regions were structurally more distinct and extended than those in polythiophene, which indicated that the fused rings underwent more easily transformation to the quinonoid forms during the geometry relaxation process than the thiophene rings. Calculated energetic aspects of the doping behavior and the spectroscopic results indicated that polaron was favored over bipolaron as the positive charge carrier, in contrast to the case of polythiophene and many other π-conjugated polymers. The conclusion that the polaron was the lowest-energy charge storage configuration indicated strong electron−electron Coulomb repulsion within the fused thiophene rings. The spins of the positive charge carriers were found at *g*-factors higher than those reported for typical π-doped conjugated polymers, indicating that the orbitals of the sulfur atoms were substantially involved in the SOMOs.

Acknowledgment. This work was partially supported by a Grant-in-Aid for Scientific Research (No. 14703029) from MEXT, Tokyo, Japan.

Supporting Information Available: Text giving synthetic methods for **DS-T$_x$** (including Scheme S1 showing the synthesis), **DS-PT**, and **MS-PT** and a figure showing the ^{1}H NMR spectra of **DS-PT**, **DSO-PT**, and **D-LPT** (Figure S1). This material is available free of charge via the Internet at http://pubs.acs.org.

References and Notes

(1) Peierls, R. E. *Quantum Theory of Solids*; Clarendon: Oxford, England, 1955.
(2) Roncali, J. *Chem. Rev.* **1997**, *97*, 173−205.
(3) *Handbook of Oligo- and Polythiophenes*; Fichou, D., Ed.; Wiley-VCH: New York, 1999.
(4) Kobayashi, M.; Chen, J.; Chung, T.-C.; Moraes, F.; Heeger, A. J.; Wudl, F. *Synth. Met.* **1984**, *9*, 77−86.
(5) Chung, T.-C.; Kaufman, J. H.; Heeger, A. J.; Wudl, F. *Phys. Rev. B* **1984**, *30*, 702−710.
(6) Hotta, S. Molecular Conductive Materials: Polythiophenes and Oligothiophenes. In *Handbook of Organic Conductive Molecules and Polymers*; Nalwa, H. S., Ed.; Wiley: Chichester, England, 1997; Vol. 2, pp 309−387.
(7) Ziegler, C. Thin Film Properties of Oligothiophenes. In *Handbook of Organic Conductive Molecules and Polymers*; Nalwa, H. S., Ed.; Wiley: Chichester, 1997; Vol. 3, pp 677−743.
(8) Hong, S.-Y.; Marynick, D. S. *Macromolecules* **1992**, *25*, 4652−4657.
(9) Brédas, J. L. *Synth. Met.* **1987**, *17*, 115−121.
(10) Wudl, F.; Kobayashi, M.; Heeger, A. J. *J. Org. Chem.* **1984**, *49*, 3382−3384.
(11) Kobayashi, M.; Colaneri, N.; Boysel, M.; Wudl, F.; Heeger, A. J. *J. Chem. Phys.* **1985**, *82*, 5717−5723.
(12) Lazzaroni, R.; Riga, J.; Verbist, J.; Brédas, J. L.; Wudl, F. *J. Chem. Phys.* **1988**, *88*, 4257−4262.
(13) Poplawski, J.; Ehrenfreund, E.; Schaffer, H.; Wudl, F.; Heeger, A. J. *Synth. Met.* **1989**, *28*, C539−C544.
(14) Meng, H.; Wudl, F. *Macromolecules* **2001**, *34*, 1810−1816.
(15) Brédas, J. L.; Thémans, B.; Fripiat, J. G.; André, J. M.; Chance, R. R. *Phys. Rev. B* **1984**, *29*, 6761−6773.
(16) Brédas, J. L.; Chance, R. R.; Silbey, R. *Phys. Rev. B* **1982**, *26*, 5843−5854.
(17) Brédas, J. L.; Heeger, A. L.; Wudl, F. *J. Chem. Phys.* **1986**, *85*, 4673−4678.
(18) Brédas, J. L. *J. Chem. Phys.* **1985**, *82*, 3808−3811.
(19) Kwon, O.; McKee, M. L. *J. Phys. Chem. A* **2000**, *104*, 7106−7112.
(20) Tachibana, M.; Tanaka, S.; Yamashita, Y.; Yoshizawa, K. *J. Phys. Chem. B* **2002**, *106*, 3549−3556.
(21) Pomerantz, M.; Gu, X.; Zhang, S.-X. *Macromolecules* **2001**, *34*, 1817−1822.
(22) Neef, C. J.; Brotherston, I. D.; Ferraris, J. P. *Chem. Mater.* **1999**, *11*, 1957−1958.
(23) Sotzing, G. A.; Lee, K. *Macromolecules* **2002**, *35*, 7281−7286.
(24) Cravino, A.; Neugebauer, H.; Luzzati, S.; Catellani, M.; Petr, A.; Dunsch, L.; Sariciftci, N. S. *J. Phys. Chem. B* **2002**, *106*, 3583−3591.
(25) Collard, D. M.; Inaoka, S. *J. Mater. Chem.* **1999**, *9*, 1719−1725.
(26) Pomerantz, M. Low Band Gap Conducting Polymers. In *Handbook of Conducting Polymers: Second Edition, Revised and Expanded*; Skotheim, T. A., Elsenbaumer, R. L., Reynolds, J. R., Eds.; Marcel Dekker: New York, 1998; pp 277−309.
(27) Rajca, A.; Wang, H.; Pink, M.; Rajca, S. *Angew. Chem., Int. Ed. Engl.* **2000**, *39*, 4481−4483.
(28) Tsuchida, E.; Oyaizu, K. *Bull. Chem. Soc. Jpn.* **2003**, *76*, 15−47.
(29) Oyaizu, K.; Mikami, T.; Mitsuhashi, F.; Tsuchida, E. *Macromolecules* **2002**, *35*, 67−78.
(30) Oyaizu, K.; Mitsuhashi, F.; Tsuchida, E. *Macromol. Chem. Phys.* **2002**, *203*, 1328−1336.
(31) Miyatake, K.; Hay, A. S.; Mitsuhashi, F.; Tsuchida, E. *Macromolecules* **2001**, *34*, 2385−2388.
(32) Haryono, A.; Miyatake, K.; Natori, J.; Tsuchida, E. *Macromolecules* **1999**, *32*, 3146−3149.
(33) Stewart, J. J. P. *J. Comput. Chem.* **1989**, *10*, 209−220.
(34) Hutchison, G. R.; Ratner, M. A.; Marks, T. J. *J. Phys. Chem. A* **2002**, *106*, 10596−10605.
(35) Karpfen, A.; Kertesz, M. *J. Phys. Chem.* **1991**, *95*, 7680−7681.
(36) Jürimäe, T.; Strandberg, M.; Karelson, M.; Calais, J.-L. *Int. J. Quantum Chem.* **1995**, *54*, 369−379.
(37) Jones, D.; Guerra, M.; Favaretto, L.; Modelli, A.; Fabrizio, M.; Distefano, G. *J. Phys. Chem.* **1990**, *94*, 5761−5766.
(38) Bakhshi, A. K. *J. Chem. Phys.* **1992**, *96*, 2339−2346.
(39) Bakhshi, A. K.; Ladik, J.; Seel, M. *Phys. Rev. B* **1987**, *35*, 704−712.
(40) Chung, T.-C.; Kaufman, J. H.; Heeger, A. J.; Wudl, F. *Phys. Rev. B* **1984**, *30*, 702−710.
(41) Brédas, J. L.; Elsenbaumer, R. L.; Chance, R. R.; Silbey, R. *J. Chem. Phys.* **1983**, *78*, 5656−5662.
(42) Karpfen, A.; Ehrendorfer, C. *J. Phys. Chem.* **1994**, *98*, 7492−7496.
(43) Cornil, J.; Beljonne, D.; Brédas, J. L. *J. Chem. Phys.* **1995**, *103*, 842−849.
(44) Hirooka, M.; Doi, T. *Synth. Met.* **1987**, *17*, 209−214.
(45) Hotta, S.; Shimotsuma, W.; Taketani, M.; Kohiki, S. *Synth. Met.* **1985**, *11*, 139−157.
(46) McCullough, R. D.; Lowe, R. D.; Jayaraman, M.; Anderson, D. L. *J. Org. Chem.* **1993**, *58*, 904−912.
(47) McCullough, R. D.; Williams, S. P. *J. Am. Chem. Soc.* **1993**, *115*, 11608−11609.
(48) McCullough, R. D. *Adv. Mater.* **1998**, *10*, 93−116.
(49) Brédas, J. L.; Street, G. B.; Thémaus, B.; André, J. M. *J. Chem. Phys.* **1985**, *83*, 1323−1329.
(50) Kofranek, M.; Kovář, T.; Lischka, H.; Karpfen, A. *J. Mol. Struct.* **1992**, *259*, 181−198.
(51) Champagne, B.; Mosley, D. H.; André, J. M. *J. Chem. Phys.* **1994**, *100*, 2034−2043.
(52) Villar, H. O.; Otto, P.; Dupuis, M. *Synth. Met.* **1993**, *59*, 97−110.

(53) Wu, X.; Chen, T.-A.; Rieke, R. D. *Macromolecules* **1995**, *28*, 2101−2102.
(54) Wu, X.; Chen, T.-A.; Rieke, R. D. *Macromolecules* **1996**, *29*, 7671−7677.
(55) Bäuerle, P.; Götz, G.; Synowczyk, A.; Heinze, J. *Liebigs Ann.* **1996**, 279−284.
(56) Yamamoto, K.; Kobayashi, S.; Shouji, S.; Tsuchida, E. *J. Org. Chem.* **1996**, *61*, 1912−1913.
(57) Yamamoto, K.; Shouji, E.; Suzuki, F.; Kobayashi, S.; Tsuchida, E. *J. Org. Chem.* **1995**, *60*, 452−453.
(58) Tak, Y.-H.; Bässler, H.; Leuninger, J.; Müllen, K. *J. Phys. Chem. B* **1998**, *102*, 4887−4891.
(59) Tak, Y.-H.; Mang, S.; Greiner, A.; Bässler, H.; Pfeiffer, S.; Hörhold, H.-H. *Acta Polym.* **1997**, *48*, 450−454.
(60) Pommerehne, J.; Vestweber, H.; Guss, W.; Mahrt, R. F.; Bässler, H.; Porsch, M.; Daub, J. *Adv. Mater.* **1995**, *7*, 551−554.
(61) Uckert, F.; Setayesh, S.; Müllen, K. *Macromolecules* **1999**, *32*, 4519−4524.
(62) Yamamoto, T.; Morita, A.; Miyazaki, Y.; Maruyama, T.; Wakayama, H.; Zhou, Z.; Nakamura, Y.; Kanbara, T.; Sasaki, S.; Kubota, K. *Macromolecules* **1992**, *25*, 1214−1223.
(63) McCullough, R. D.; Lowe, R. D. *J. Chem. Soc., Chem. Commun.* **1992**, 70−72.
(64) Colaneri, N.; Nowak, M.; Spiegel, D.; Hotta, S.; Heeger, A. J. *Phys. Rev. B* **1987**, *36*, 7964−7968.
(65) Sebti, M.; Merlin, A.; Ghanbaja, J.; Billaud, D. *Synth. Met.* **1997**, *84*, 665−666.
(66) Alberti, A.; Favaretto, L.; Seconi, G. *J. Chem. Soc., Perkin Trans. 2* **1990**, 931−935.
(67) Bäuerle, P.; Segelbacher, U.; Gaudl, K.-U.; Huttenlocher, D.; Mehring, M. *Angew. Chem., Int. Ed. Engl.* **1993**, *32*, 76−78.

MA030520P